Quantification of non-Newtonian fluid dynamics of a wormlike micelle solution in porous media with magnetic resonance

Authors: Jennifer R. Brown, Jacob Trudnowski, Elmira Nybo, Katherine E. Kent, Thomas Lund, and Amanda Parsons

Brown J.R., J. Trudnowski, E. Nybo, K.E. Kent, T. Lund, A. Parsons, "Quantification of non-Newtonian fluid dynamics of a wormlike micelle solution in porous media with magnetic resonance," Chemical Engineering Science 173, (December 2017):145-152.

Quantification of non-Newtonian fluid dynamics of a wormlike micelle solution in porous media with magnetic resonance

Jennifer R. Brown *, Jacob Trudnowski, Elmira Nybo, Katherine E. Kent, Thomas Lund, Amanda Parsons

Keywords:
Magnetic resonance
PGSE NMR
Wormlike micelles
Fracturing fluids
Porous media

Nuclear magnetic resonance (NMR) pulsed gradient stimulated echo (PGStE) techniques were used to observe anomalous transport phenomena for flow of a non-Newtonian wormlike micelle solution through a model porous media. Understanding the flow behavior of wormlike micelle solutions in porous media is important due to the growing interest of these solutions in enhanced oil recovery. NMR velocity imaging was unable to discern differences in the flow field between shear-thickening wormlike micelle solution and water due to spatial resolution limitations. However, the probability of displacement, i.e. the propagator, was skewed towards slower velocities and long tails at high displacements for the micelle solution and incorporation of a fractional dynamics approach using the moments of the probability dis-tribution showed a deviation from asymptotic Gaussian statistics.

Surfactants can self-assemble in solution at certain tempera-tures and concentrations to form meso-structures, or micelles. Micelles are used in various applications including personal and home care products and as drag reduction agents (Yang, 2002; Chu et al., 2013). A particular class of micelles that form long cylin-drical structures, i.e. wormlike micelles, have become of interest as hydraulic fracturing fluids in oil recovery (Maitland, 2000; Ezrahi et al., 2006; Golombok and van der Wijst, 2013; van Santvoort and Golombok, 2016; Barbati et al., 2016). Low reservoir perme-ability can severely limit oil production. Often polymeric fluids are used to transmit hydraulic pressure to the rock formation, cre-ating fractures that are kept open by small particles such as sand transported into the fractures. However, cross linked gels used in this process must eventually be degraded. Any remaining gel struc-ture can reduce permeability, and therefore the oil recovery effi-ciency. Wormlike micelles are of growing interest as fracturing fluids due to their unique viscoelastic fluid properties.

When these surfactants come into contact with hydrocarbons, they revert back to spherical micelles, decreasing the fluid viscosity dramatically and allowing it to flow easily from the fractures (Maitland, 2000). While there is much current work being done to characterize the complicated rheological characteristics of wormlike micelle solutions (Huang et al., 2009), their behavior in porous media flows is still largely unexplored. Complex fluids under deformation can exhibit both space and time dependencies, and in combination with the multiple length scales inherent to porous media, fluid flow behavior is difficult to predict. Models have attempted to incorporate non-Newtonian fluid effects into an effective viscosity (Pearson and Tardy, 2002) as well as network and macroscopic models valid typically for shear-thinning fluids (Balhoff and Thompson, 2006; Lopez et al., 2003; Chaplain et al., 1998). Typical experimental studies measure pressure drop as a function of flow rate (Chhabra et al., 2001), in order to measure the resistance to flow due to the porous medium. The challenge is then to relate this bulk pressure drop to complex fluid properties. Muller et al. (1998) found for a viscoelastic fluid in porous media a critical stress corresponding to an onset of increased flow resistance, correlated with

fluctuations in velocity and spatial position, termed elastic instabilities in relation to flow irregularities observed above a critical value of the Weissenberg number (>1). In a porous medium, both shear and extensional forces are important and for semi-flexible polymers shear effects dominated at low Reynolds numbers resulting in a decrease in the resistance function with increasing flow rate (Gonzalez and et al., 2005). At higher Reynolds numbers, increased resistance occurred as extensional components of the flow dominated. Similar effects could be expected for self-assembling micelle structures, although this has not been explored extensively in the literature. Muller et al. (2004) did measure extensional viscosities for shear-thickening cetyltrimethylammonium p-toluenesulfonate (CTAT) via opposed jet flow measurements. They found no enhancement in extensional viscosity over that of water for dilute concentrations (<0.23 wt%) and enhanced extensional viscosity but no extensional thickening for higher concentrations. However, an enhanced viscosity or resistance was observed for flow in a porous media at all concentrations that was markedly larger and occurred at lower flowrates than would be expected from the shear rheology alone, presumably due to elongational effects on shear-induced structures (Muller et al., 2004; Rojas et al., 2008).

Non-invasive and non-destructive Magnetic Resonance (MR) techniques, however, can monitor macroscopic phenomena such as the spatially resolved flow field and full probability distributions of displacement in opaque porous media, instead of relying upon bulk pressure drop. MR velocity imaging can map fluid velocity, providing micron scale spatial resolution of the flow field (Fukushima, 1999; Callaghan, 1991), while Pulsed Gradient Spin Echo (PGSE) MR techniques can measure diffusion or dispersion (Stejskal and Tanner, 1965) in porous media as well as provide a link between macroscopic generalized transport phenomena and microscopic dispersion (Seymour and Callaghan, 1997; Seymour and Callaghan, 1996; Seymour and et al., 2004; Callaghan and et al., 1992; Callaghan and et al., 1991; Hunter and Callaghan, 2007). Through direct imaging of preferential flow paths (Sheppard et al., 2002), measurement of the probability distribution of fluid displacement (the propagator) in the pore space due to flow (Seymour and Callaghan, 1997), dispersion measurements (Seymour and et al., 2004; Stapf and et al., 1998) and diffusive diffraction type analysis at the pore scale (Seymour and Callaghan, 1997; Seymour and Callaghan, 1996; Callaghan and et al., 1991), the dynamics of fluid flow through porous media can be well-characterized (Manz et al., 1999). Most recently, Scheven et al. (2007) measured intrinsic dispersion coefficients for non-inertial flow through random porous media which agree with Saffman's capillary model (Saffman, 1960) and LB simulations (Maier and et al., 2000). Manz et al. (1999) used 3D MRI to obtain pore structure information directly inputted into LB simulations, finding good quantitative agreement for flow visualization and dispersion over a range of Peclet and Reynolds numbers in model porous media. PGSE MR measurements of the displacement propagator in a model porous media were used to observe the evolution from Gaussian statistics to anomalous transport processes due to the growth of biofilm and resultant alterations of the pore space (Seymour and et al., 2004). Guillon et al. (2013) analyzed the variance of the displacement propagator as a function of observation time to quantify asymptotic non-Gaussian statistics in unsaturated porous media. These abilities have demonstrated MR as a preeminent technique for porous media analysis over the last two decades (Seymour and Callaghan, 1997; Callaghan, 2011; Song and et al., 2008).

For non-Newtonian fluids in porous media, the body of MR experimental work is not large. Cumulant analysis (Kubo et al., 1991) has been applied to non-Gaussian propagators measured for flows in porous media and rock (Scheven and et al., 2007), implying enhanced dispersion over water for flow of a shear-thinning xantham gum solution. Mertens and et al. (2006) measured 3D MR Images, 2D velocity images and propagators for a xantham gum solution in a model porous media and observed "shear thinning" behavior as evidenced from the coincidence of the propagators. Sullivan and et al. (2007, 2006) compared 2D and 3D velocity imaging results to LB simulations for shear-thinning fluids in complex geometries to quantify the increased dispersion associated with shear-thinning fluids. Chevalier et al. (2014) used PGSE to effectively measure the velocity distribution for a yield stress fluid and found no difference in the flow field compared to Newtonian fluids. Spectrally resolved 1D MR profiles and rapid 2D imaging was used to study fracturing fluids in rock core flooding experiments (Sheppard et al., 2002). Permeability changes in rock cores after treatment with a polymer solution were investigated through changes in the propagator over time (Johns and et al., 2003).

In this work, MR velocity imaging and PGSE measurements were used to provide detailed information about the pore structure, velocity field and displacement probability distribution for a shear-thickening wormlike micelle solution of 10 mM CTAT in water flowing in a model porous media. Imaging showed no difference in the flow field of the wormlike micelle solution when compared to water. However, the probability distribution of displacement revealed anomalous diffusive dynamics.

2. Magnetic resonance

Magnetic Resonance (MR) utilizes the radio frequency excitation of active nuclei magnetic moments, in this case, the proton ^{1}H. With application of a large magnetic field B_o, the nuclei resonate at a frequency proportional to the field, $\omega_0 = \gamma B_0$ (Ernst et al., 1988) and application of a magnetic field gradient $\boldsymbol{G}$ forces the resonant frequency to depend on position $\mathbf{r}$, $\omega = \gamma(B_0 + \boldsymbol{G}.\boldsymbol{r})$. This relationship is the foundation of magnetic resonance imaging (MRI), which may be combined with measurement of translational motion or molecular dynamics.Measurement of translational motion; whether self-diffusion, coherent velocity or dispersion; again exploits the resonant frequency dependence on magnetic field variation. With the strategic application of a pair of rectangular narrow gradient pulses of amplitude g, duration δ and separation Δ, the pulsed gradient spin echo (PGSE) sequence, displacement is encoded (Callaghan, 1991; Seymour and Callaghan, 1997; Stepisnik, 1985). For narrow gradient pulses, the acquired signal gives the conditional probability that a molecule will be displaced by a distance $R = r - r'$ over a time Δ,

$$\bar{P}_s(R,\Delta) = \int \rho(r) P_s(r|r',\Delta) dr \cdot P_s(r|r',\Delta) \tag{1}$$

The signal may be sensitized to measure translational motion over a range of displacements from 10 nm to 1 mm on timescales from 100 μs to 1 s. Spatial encoding can be combined with PGSE encoding of motion to obtain a signal modulation resulting in a time averaged velocity for each image voxel, a velocity image. MR Imaging of the flow field has been applied extensively in complex spatial geometries such as porous media (Fukushima, 1999; Seymour and et al., 2004; Sederman and et al., 1997), but also for complex fluid characterization in Rheo-NMR applications (Feindel and Callaghan, 2010; Britton and Callaghan, 1997; Cokelet and et al., 2005). PGSE NMR has also been used extensively to measure diffusion and dispersion (Seymour and Callaghan, 1997; Hunter and Callaghan, 2007; Manz et al., 1999; Amin and et al., 1997; Codd and et al., 1999; Khrapitchev and Callaghan, 2003). For random Brownian motion, where the propagator follows a Gaussian

distribution, the normalized NMR signal attenuation is related to the diffusion coefficient via the Stejskal-Tanner relationship (Callaghan, 1991; Stejskal and Tanner, 1965)

$$E(q,\Delta) = S(q,\Delta)/S(0,\Delta) = \exp[-q^2 D(\Delta - \delta/3)] \quad (2)$$

where $q = \gamma\delta g/2\pi$ and D is the diffusion coefficient and assumed to vary linearly with the mean squared displacement via the standard Einstein definition $\langle r^2\rangle = 2D\Delta$. Even when the underlying propagator is not Gaussian, the signal attenuation in the low q limit is related to the mean squared displacement, which is the variance of the probability distribution (Callaghan, 1991; Guillon and et al., 2014)

$$\ln|E(q,\Delta)| = -\frac{1}{2}\sigma^2 q^2 \quad (3)$$

3. Materials and methods

3.1. Sample preparation

Hexadecyltrimethylammonium p-toluenesulfonate (CTAT) dry powder (Sigma Life Science) was mixed with de-ionized water to create wormlike micelle solutions with concentrations ranging from 1 mM to 30 mM. Solutions were placed in a water bath at 25.0 °C, above the Kraft temperature of 22.5 °C, and allowed to equilibrate for 24 h before use in rheology and MR experiments. Magnevist ® was added at 0.085% concentration to decrease the spin-lattice (T_1) relaxation time of the samples to ~2 s for faster acquisition in NMR PGSE measurements.

3.2. Model porous media

A model porous medium was constructed using a 10 mm ID high performance liquid chromatography column (Omni-fit) of 50 mm length. The column was wet packed with 235 μm monodisperse dry polymer microspheres (Duke Standards, Thermo Scientific). The polymer microspheres have low susceptibility differences from the fluid (the spectral linewidth in the NMR experiments was ~600 Hz), minimizing any variations in the magnetic field and possible associated susceptibility artifacts. A Pharmacia P-500 high precision pump was used to pump fluid through the microsphere bead pack against gravity at a controlled volumetric flowrate. The microsphere bead pack was flushed with fluid for at least 12 h prior to running MR experiments in order to eliminate air bubbles within the system. Active temperature control was not employed within the MR spectrometer. Therefore, to maintain the necessary 25 °C in CTAT during acquisition of MR data, the beaker of CTAT solution was kept in a water bath and the temperatures of both the surrounding room and the cooling water flowing through the magnetic gradient set were set to 25 °C.

3.3. Rheology

Rheological measurements were conducted at 25 °C with an AR-G2 rheometer (TA Instruments) equipped with a 60 mm diameter stainless steel parallel plate geometry and 60 mm diameter cone-and-plate with a 2° cone angle. Temperature was controlled to within 0.1 °C by a Peltier plate. Flowcurves were collected under a controlled strain for shear rates ranging from 1 to 1000 s^{-1}.

3.4. MR methods

All MR measurements were performed with a Bruker AVANCE III spectrometer with a 7 T superconducting vertical wide bore magnet, Micro2.5 gradient imaging probe capable of producing maximum gradients of 1.48 T m^{-1} and 25 mm diameter radiofrequency (r.f.) coil. Standard pulse gradient stimulated echo (PGStE) pulse sequences were used (Callaghan, 1991), due to the short T_2 times present in porous media, to acquire probabilities of spin displacement and effective dispersion coefficients. For the PGStE propagator measurements, the echo time (TE), the total time in the x-y plane, was 4.3 ms, the δ was 1 ms and Δ ranged from 300 ms to 850 ms. For PGStE measurements of dispersion coefficients, the δ was 0.3 ms and Δ ranged from 1300 ms to 1900 ms with a TE = 4.3 ms. Standard velocity imaging sequences were used to acquire velocity images (Callaghan, 1991). NMR parameters for the velocity images were: δ = 0.5 ms, Δ = 9 ms and TE = 14.8 ms. Images had a spatial resolution of 47 × 47 μm (FOV = 12 × 12 mm and matrix size 256 × 256) over a 0.5 mm slice thickness.

4. Results

Surfactants that self-assemble into long cylindrical polymer-like molecular structures, "wormlike" micelles, exhibit complex viscoelastic behavior; including shear-thinning, shear-thickening and shear banding instabilities (Berret et al., 2006). For the wormlike micelle solution used in this study (CTAT) self-assembly of spherical micelles occurs at the critical micelle concentration (CMC) of 0.26 mM at 25 °C. At the critical rod-like concentration (CRC) of 1.9 mM (25 °C), the micelles grow to form long cylindrical, or wormlike, micelles (Lerouge et al., 2010). Previous studies have shown that at concentrations below the CRC, the viscosity is Newtonian, while at concentrations above the CRC, both shear-thickening and shear-thinning occurs depending on applied shear rate (Lerouge et al., 2010; Berret et al., 2002). For a 10 mM concentration (Fig. 1), shear-thickening occurs at an intermediate applied shear rate of approximately 40 s^{-1} due to the formation of shear-induced structures (SIS) and growth of the micelle length (Lerouge et al., 2010), while above an applied shear rate of 130 s^{-1} micelles begin to align in the velocity field, causing shear-thinning. If the concentration were increased above the overlap concentration, entanglements would result and the rheology would exhibit an elevated zero shear viscosity and a shear-thinning that occurs with increasing shear rate as cooperative structures are formed and micelles align. The concentration of 10 mM CTAT was chosen for flow through the porous media due to the high degree of shear-thickening that occurs at intermediate shear rates under simple shear. For the NMR measurements conducted here, a doping agent (Magnevist ®), a salt of a complex of gadolinium (Gd^{3+}) with diethylenetriaminepentacetate ($DTPA^{5-}$),

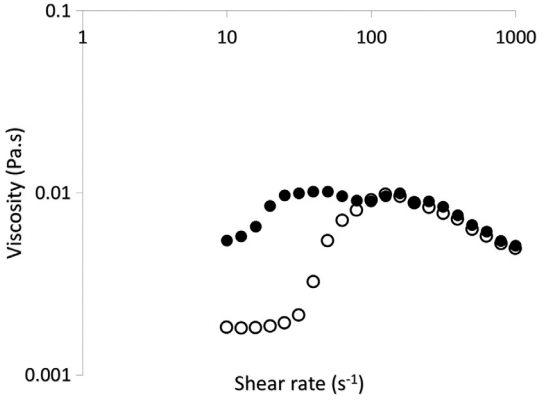

Fig. 1. Apparent viscosity of 10 mM CTAT in water (open circles) and 10 mM CTAT in water doped with 0.085% Magnevist (closed circles). An enhancement of the low shear rate viscosity and earlier onset of shear thickening behavior is observed with the addition of the gadolinium salt complex.

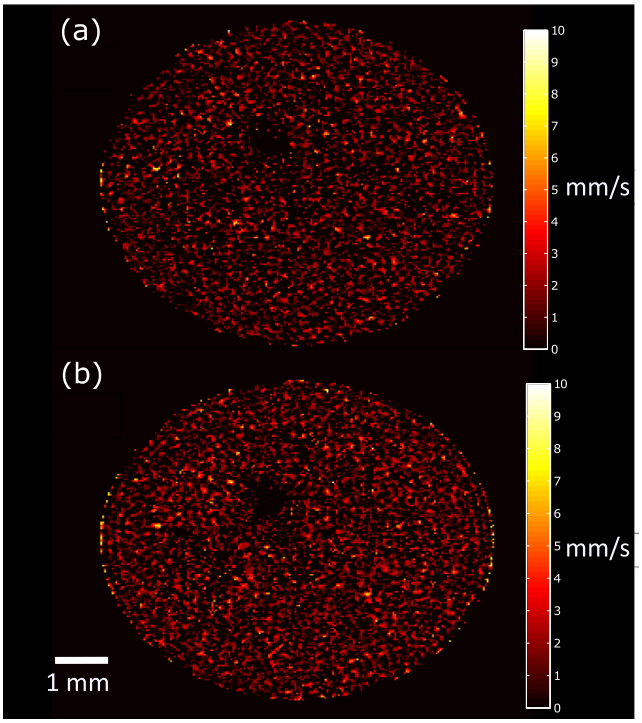

Fig. 2. Cross-sectional velocity images showing velocity along the main direction of flow (z) for a volumetric flowrate of 400 ml/h. Spatial resolution of 47 × 47 μm over a 0.5 mm slice. (a) Water and (b) doped 10 mM CTAT solution. The velocity images at this spatial resolution indicate that the fluid rheology does not have a large impact on the velocity field and that the porous structure dominates.

was added to reduce the spin-lattice (T_1) relaxation time of the samples and therefore the overall acquisition time of the experiments. The addition of the doping agent to the 10 mM solution caused an increase in viscosity at low shear rates and the onset of shear-thickening to occur at lower shear rates (~20 s^{-1}; Fig. 1). An increase in the amount of transience, viscosity that changed with time at a fixed shear rate, was also observed in the shear-thickening regime. Presumably, the presence of the gadolinium complex is stabilizing the micelle structure and causing further growth of SIS under shear.Both water and the doped 10 mM CTAT solution was flowed through a packed bed of 235 μm diameter monodisperse polystyrene spheres at a flowrate of 400 ml/hr, corresponding to a tube, or superficial, velocity $\langle v_{tube} \rangle = v_s = Q/A$ of 1.42 mm s^{-1}. From the propagator measurement for water (Fig. 3), the average velocity $\langle v \rangle$ within the pores of the microsphere bead pack was 2.88 mm/s. As $\langle v \rangle = v_{pore} = \langle v_{tube} \rangle / \phi$, the liquid volume fraction ϕ in the microsphere bead pack is approximately 0.49. Due to the presence of the solid spheres and resultant changing cross-sectional area in the direction of flow, there is a distribution of shear rates within the porous medium. However, the apparent shear rate can be defined as $\dot{\gamma}_{app} = \langle v \rangle / l = \langle v \rangle (1-\phi)/d_p\phi$ for spheres; where l is a characteristic length scale equal to $d_p\phi/(1-\phi)$ for spheres and d_p is the microsphere diameter. The apparent shear rate was calculated as 12 s^{-1}. From viscosity measurements for 10 mM CTAT in Fig. 1, an apparent shear rate of 12 s^{-1} would fall at the beginning of the shear-thickening regime where SIS begin to form. This viscosity is measured under simple shear conditions without extensional components as are present in flow through porous media. The shear rate also varies substantially within the porous media and

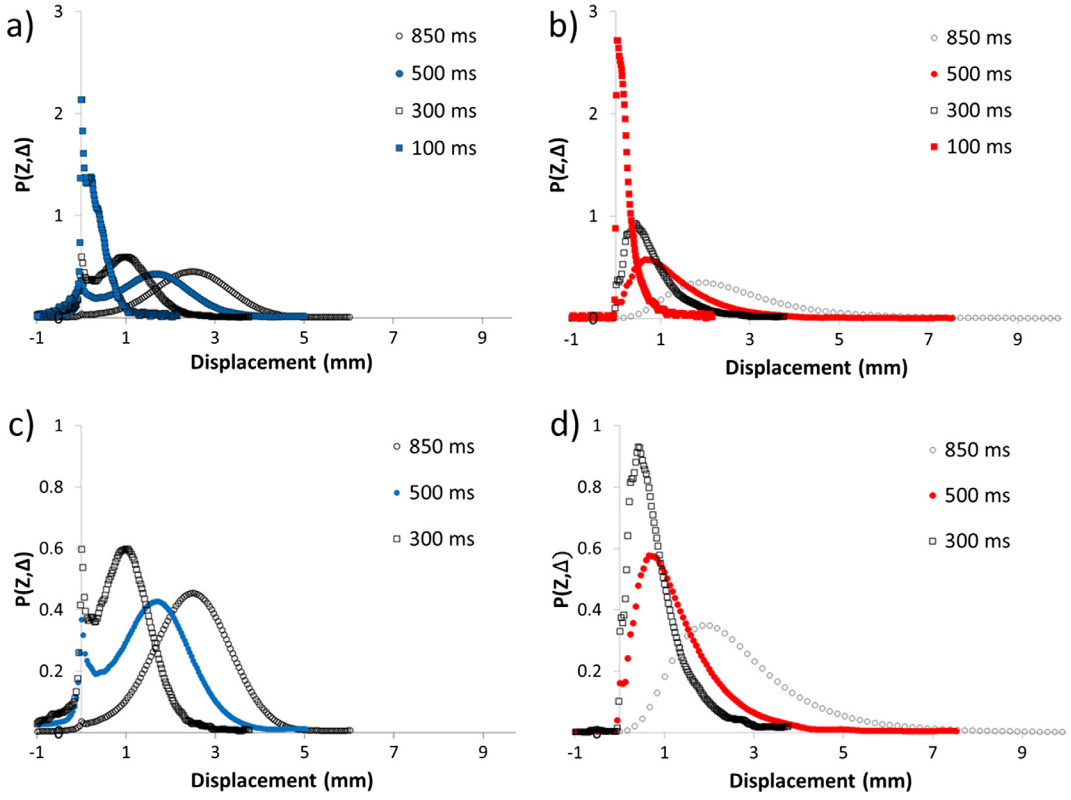

Fig. 3. Propagators for a volumetric flowrate of 400 ml/h as a function of observation time. (a) Water at all observation times, (b) 10 mM CTAT at all observation times, (c) water for selected observation times of 300 ms, 500 ms and 850 ms, demonstrating the evolution to Gaussian behavior and (d) 10 mM CTAT for selected observation times, showing a non-Gaussian distribution with high displacement long tails.

therefore there would be regions with varying amounts of shear-thickening behavior. At this flowrate, the Reynolds number $\mathrm{Re} = \langle v \rangle d_p / \nu$, calculated here based on the properties of water, is low at 0.81. In the low Reynolds number regime ($\mathrm{Re} < 1$), inertial effects are negligible. The Peclet number for water $Pe = \langle v \rangle d_p \phi / D_o (1 - \phi)$, where D_o is the water self-diffusion coefficient (=2.34×10^{-9} m^2 s^{-1} at 25 °C), is 291. The Peclet number relates the relative importance of advection to diffusion.

Fig. 2 shows cross-sectional 2D NMR velocity images where velocity is measured in the main direction of flow (z). As indicated in the colorbar, black corresponds to regions of zero velocity (generally where the solid microspheres are located) with lighter colors corresponding to faster velocities. The velocity image for 10 mM CTAT at 400 ml/hr (Fig. 2b) shows a very similar flow distribution spatially throughout the microsphere bead pack as for water (Fig. 2a). The average velocity within the microsphere bead pack for CTAT was 2.60 mm/s, very similar to the 2.49 mm/s measured for water (percent error ~4%), as would be expected for a fixed volumetric flowrate, where the average velocity should be the same for the two fluids regardless of changes to the flow field due to fluid rheology.

The velocity images indicate that the fluid rheology does not have a large impact on the velocity field and that the porous structure dominates. Previous MR velocity imaging measurements of shear thinning fluids in porous media have shown deviations in the flow field due to the non-Newtonian character of the fluid. Mertens et al. (2006) observed a non-coincidence of normalized velocity distribution curves obtained from spatially resolved velocity maps for 0.5% xanthan gum solution flowing in a packed bed of 1.7 mm and 4 mm diameter spheres. Sullivan et al. compared MR velocity imaging results for two shear-thinning polymers, carboxyl methyl cellulose and polyacrylamide, flowing in a 5 mm diameter sphere pack to lattice-Boltzmann simulations incorporating an apparent viscosity (Sullivan and et al., 2007). These studies utilized large sphere diameters, and therefore pore sizes, in order to achieve sufficient spatial resolution to resolve small changes in velocity due to non-Newtonian fluid properties. The microsphere diameter for the velocity imaging data shown in Fig. 2 was 235 μm and so the approximate pore diameter is 235 μm. With a spatial resolution of 47×47 μm, that results in ~5 pixels across a pore diameter. In addition, the velocity images are averaged over a 0.5 mm slice and therefore the velocity in a pixel is averaged over ~2 microsphere diameters. It is possible that the non-Newtonian character of the fluid is not easily observed at these spatial resolutions, emphasizing that caution needs to be used for spatially resolved techniques. However, non-spatially resolved PGSE NMR measurements of the probabilities of displacement, the propagator, can provide more detailed information about the statistics of the flow field.

In Fig. 3(a), propagators are plotted for increasing observation times from 100 to 850 ms with a constant echo time of 4.3 ms for water flowing at 400 ml/hr through the model bed of packed microspheres. At short times, a spike at zero displacement is observed. With increasing observation time, there is an evolution from preasymptotic behavior towards asymptotic Gaussian behavior, as expected in the long time limit. The resulting probabilities of displacement in the asymptotic regime for homogeneous media are expected to exhibit Gaussian statistics centered about the average velocity (Seymour and Callaghan, 1997; Guillon et al., 2013).

Fig.3(c) shows propagators for just the longer observation times (300, 500 and 850 ms) for water. The propagator for water at 850 ms observation time is largely Gaussian with only a small zero displacement peak. Depending upon the packing of each individual microsphere bead pack (loaded with exactly the same procedure), the zero displacement peak can be more or less pronounced for each experimental run, presumably due to the presence or absence of stagnation zones with small variations in the random packing. Negative displacements can occur due to diffusion of molecules in stagnation zones. In this case, the zero displacement peak is nearly absent at 850 ms observation time and is therefore expected to have a negligible impact on the signal for experiments with longer observation times.

For the 10 mM CTAT solution however (Fig.3(b) and (d)), the evolution towards Gaussian is significantly slower with a skewing of the propagator towards zero displacement. In addition, a high displacement long tail is observed that is not present in the water propagator. These features clearly indicate the impact that the presence of wormlike micelles formed from the CTAT molecules have on the transport dynamics in the porous medium.

Long tails in the probability distribution have been observed and would be expected for flow of a shear-thinning polymer solution in porous media (Mertens and et al., 2006). As the fluid moves through the pore space, it experiences a range of apparent shear rates, presumably higher near the solid boundary of the spheres and nearing zero at the center of the pore. For a shear-thinning fluid, a higher shear rate reduces viscosity. In capillary flow, the result is a velocity profile that becomes more plug-like. For a shear-thickening fluid, a higher shear rate would result in an increase in viscosity, essentially a stiffening of the fluid and increased resistance to flow. In capillary flow, the result is a sharpened velocity profile from parabolic. For flow of a shear-thickening CTAT solution in porous media, there are additional effects that may also impact the flow dynamics.

In these experiments, the CTAT micelles are cationic and the model microsphere pack consists of polystyrene microspheres with a slight negative charge. Therefore surface interactions could be present, but are not likely to be strong as the surface charge on the microspheres is small. Additional research would be needed to quantify the impact of surface interactions in this system. In addition, there is the possibility of shear-induced structure formation, as observed in CTAT solutions under simple shear. Either of these effects could result in viscosity varying across the pore.

Elongational forces are also present in porous media due to the changing cross sectional area available for flow. As extensional viscosities of polymers are often much higher than shear viscosity at low shear rates (Sridhar and et al., 1991), elongational forces are likely to have a strong impact on flow in porous media. Previous work for shear-thinning polymer solutions flowing in porous media has indicated an early onset of increased resistance to flow over that expected from the shear viscosity (Gonzalez and et al., 2005). Presumably this is due to stiffening of the polymers under elongation, although it is difficult to discern experimentally the source of increased resistance, whether extensional stiffening, mechanical retention or other mechanisms (Gonzalez and et al., 2005). Odell and Haward observed increased viscosity enhancement for packed beds with stagnation points over those without, attributed to a coil-stretch transition of the polymer chains (Odell and Haward, 2006). Studies of wormlike micelle solutions under extensional forces are somewhat sparse, however, thickening has been observed under extension in an opposed jet device for wormlike micelle solutions known to exhibit shear-thinning under simple shear (Prudhomme and Warr, 1994; Walker et al., 1996; Fischer et al., 1997; Lu and et al., 1998) and strong extensional thickening was observed in capillary breakup experiments (Yesilata et al., 2006). At high extension rates, the extensional viscosity has been seen to drop, an effect hypothesized to be due to micellar scission (Chen and Warr, 1997; Rothstein, 2003). Elastic instabilities have been observed for an entangled wormlike micelle solution under extensional flow in a microfluidic cross-slot device (Haward and et al., 2012) and for flow around confined microfluidic cylinders (Zhao et al., 2016).

In the case of CTAT solutions, extensional viscosity obtained via opposed jet flow measurements did not show extensional thickening for dilute and semi-dilute concentrations (Muller et al., 2004). However, an increased resistance to flow (quantified as an increased flowrate under constant pressure drop) was observed for shear-thickening CTAT solutions when flowing in porous media (Muller et al., 2004; Rojas et al., 2008). While considered a "shear-thickening" effect, the increased resistance to flow occurred even at dilute concentrations and was observed at lower apparent shear rates than the shear-thickening behavior seen in simple shear. Muller et al. (2004) hypothesize this increased resistance was because of the formation of SIS, due to the shear component of the flow, which then allowed the extensional component of the flow to cause an enhancement of extensional viscosity not observed in conditions of pure extension. The NMR PGSE propagator measurements are consistent with this scenario, as increased resistance to flow due to shear forces alone (i.e. the shear-thickening behavior observed in rheological measurements of Fig. 1) would not explain the presence of long tails in the probability distribution at large displacements.

To quantify the deviation from non-Gaussian statistics in the propagators and therefore differences in transport behavior between Newtonian water and shear-thickening CTAT, we can calculate the moments of the probability distributions. At the longest observation time (850 ms), the average displacement, or first moment of the probability distribution, is 2.45 mm and 2.67 mm for water and CTAT respectively. The average velocities therefore are 2.88 mm s^{-1} and 3.14 mm s^{-1}respectively. The discrepancy between the average velocities measured from the velocity images and the propagators could be due to variations in the packing within one 0.5 mm slice (for the velocity images) and the entire 20 mm bead pack length (for the propagator measurements) or due to the different relaxation weighting between the two types of experiments (echo time of 14.8 ms for velocity images versus 4.3 ms for propagators).

The third moment of the distribution is skew, which quantifies any asymmetry in the distribution. The skew for water at 850 ms is 0.8, indicating that the observation time is not quite long enough for the flow to fully exhibit Gaussian statistics. However, the skew for 10 mM CTAT at the same observation time is 2.1, confirming that the clearly visible slanting of the distribution towards the zero displacement in CTAT is significantly larger than for water. The statistics of the probability distributions, mean displacement and skew, give us some measure of the difference between Newtonian water and the non-Newtonian (shear-thickening) wormlike micelle solution. However, they do not explain or fully quantify the observed long tails and deviation from Gaussian behavior. Alternatively, a fractional dynamics approach may be used to quantify the deviation from Gaussian behavior observed and therefore characterize anomalous or preasymptotic transport (Metzler and Klafter, 2000). A continuous time random walk (CTRW) relates the probability for a molecule to make a jump to the wait time probability distribution w(t) and jump length distribution λ(Z). For Poisson wait time and Gaussian jump length distribution, Brownian motion is modeled and Gaussian behavior restored. Long tails in the displacement probability distribution are well-modeled using a Poisson wait time and Levy jump length to get non-Gaussian behavior. The probability distribution $P(Z)$ follows $P(Z) \approx a/Z^{1+\alpha}$ in the long displacement limit, where α is 1 for Gaussian statistics expected flow in homogeneous porous media and <2 for either anomalous asymptotic dispersion or preasymptotic non-Gaussian behavior (Metzler and Klafter, 2000; Metzler and Klafter, 2001; Shlesinger et al., 1993).In porous media that has reached the long time limit, *i.e.* the asymptotic regime where in homogeneous media Gaussian statistics are expected, one can monitor the variance of the displacement directly through the attenuation of the PGSE NMR signal in the low q limit (Eq. (3)); as opposed to measuring the full probability distribution (Guillon et al., 2013). Analysis directly in the q domain instead of the propagator space has the benefit of avoiding errors introduced through the Fourier Transform. For Gaussian behavior, this variance scales linearly with observation time. Preasymptotic, sub- or super dispersion processes can be characterized by a power law dependence of the variance with observation time $\sigma^2 \propto \Delta^{\alpha}$ (Guillon et al., 2013; Guillon and et al., 2014; Scheven and Sen, 2002; Neel et al., 2011).Fig. 4 shows σ^2 as a function of observation time for water and 10 mM CTAT. Non-Gaussian statistics can be expected for flow where anomalous transport occurs, but also in the preasymptotic flow regime, where fluid molecules have not fully sampled the pore space. In order to estimate the minimum observation time needed to reach the asymptotic limit, the criteria of Scheven and Sen (Scheven and Sen, 2002) was used. For model sphere packs, the long time limit is proposed to occur when a diffusion length $L_D = \sqrt{2D_o t} > 0.3d_p$ has been travelled, where D_o is the self-diffusion coefficient of the pore fluid, t is the timescale of the experiment (in the case of the PGSE propagator measurement, it is the observation time Δ) and d_p is the solid sphere diameter (Scheven and Sen, 2002). According to this criteria, a minimum of 1.22 s is required to be fully in the asymptotic regime. Therefore, we have sampled from 1.3 to 1.9 s, where 1.9 s is the longest time, as limited by T_1 relaxation. In addition, a constant echo time of 4.3 ms and a stimulated echo was used for all experiments, which would keep any T_2 relaxation weighting constant for all observation times sampled. A second criteria is that the average displacement be greater than $10d_p$. From the data in Fig. 3 at 850 ms observation time, the average displacement is 2.22 mm, which is nearly equal to $10d_p$ (= 0.0025 m). However, Khrapitchev and Callaghan (2003) measured the velocity autocorrelation function in porous media and found it went to zero, at which point the process should have Gaussian statistics, by $\sim 4d_p$. Therefore, by all criteria (Khrapitchev and Callaghan, 2003; Scheven and Sen, 2002) at the flowrate studied here and for the microsphere size of 235 μm, we would expect Gaussian statistics in a homogeneous bed of packed monodisperse spheres for observation times greater than 1.22 s.On a log scale, the slope of the line in Fig. 4 gives the power law exponent α. For water, $\alpha = 1.1$ ($R^2 = 0.6$) which is near the expected $\alpha = 1$ and Gaussian statistics govern the probability distribution of displacement. For CTAT however, $\alpha = 1.45$ ($R^2 = 0.91$), an indication of "super-dispersive" anomalous transport or preasymptotic transport. Although the bounds of the data

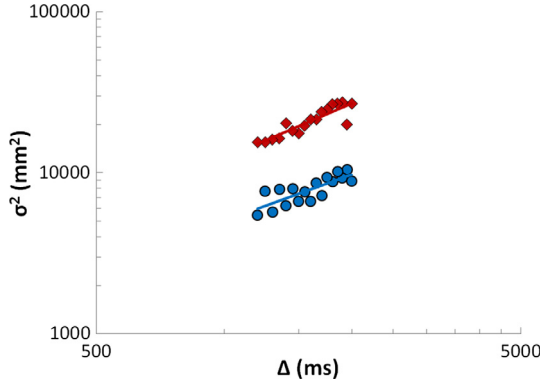

Fig. 4. Variance of the displacement as a function of observation time in the long time limit for water (circles) and 10 mM CTAT (diamonds). The power law exponent $\alpha = 1.1$ for water and $\alpha = 1.45$ for 10 mM CTAT. For water, $\alpha = 1.1$ near the expected $\alpha = 1$ and Gaussian statistics govern the probability distribution of displacement. For CTAT however, $\alpha = 1.45$, which indicates "super-dispersive" anomalous transport is occurring.

are fairly broad, the average gradient does differ significantly between the two fluids.

Seymour et al. observed a shift from Gaussian statistics in a homogeneous porous media with the growth of biofilm in the pore space (Seymour and et al., 2004), due to the biofilm creating a heterogeneous structure. Here, the shear-dependent viscosity and formation of shear-induced structures for the micellar solution under the shear and elongational forces in porous media flow could be the source of the heterogeneity, resulting in anomalous transport. Alternatively, the fluid properties could be increasing the lengthscale needed to reach the asymptotic limit. Regardless, the deviation from Gaussian statistics is an indicator of the non-Newtonian rheology of the fluid. For anomolous transport processes, where n does not equal 1, the classic scaling of dispersion with Peclet number would not be expected (Saffman, 1960; Shlesinger et al., 1993; Scheven and Sen, 2002; Neel et al., 2011). The data shown here demonstrates that the presence of wormlike micelles alters the flow through the porous media and causes anomalous dispersive behavior, making prediction of Pe scaling more complex.

5. Conclusions

Here we have observed non-Gaussian statistics in the probability of displacement, i.e. the propagator, for flow of a non-Newtonian CTAT wormlike micelle solution through a model porous media. Previous measurements for the shear-thickening micelle solution studied here indicated an increased resistance to flow within a model porous media. Using NMR PGSE velocity imaging and measurement of the propagator, data beyond bulk changes in flow rate or pressure drop were obtained; in particular, the spatially resolved flow field and transport properties. Due to spatial resolution limitations, velocity imaging was only able to discern small differences in the flow field between shear-thickening wormlike micelle solution and water. However, using PGSE NMR to measure the probability of displacement, a skewing of the probability distribution towards slower velocities and long tails at high displacements were observed for the micelle solution. Using a fractional dynamics approach, a deviation from asymptotic Gaussian statistics was found due to the non-Newtonian rheology of the wormlike micelle solution. The results re-emphasize that rheological measurements under simple shear conditions or pure extension do not fully predict or capture the complicated fluid dynamics of a shear-thickening solution in porous media. Further research would be needed to discern the microscopic mechanisms behind the anomalous transport in this system and much work is still needed in general for non-Newtonian fluid flows in porous media. However, the results presented here demonstrate the powerful potential of NMR in this field and the wealth of information to be gained from analyzing the statistics of displacement probability distributions measured with NMR PGSE.

Acknowledgements

The authors acknowledge Sarah L. Codd and Joseph D. Seymour for helpful discussions. Acknowledgment is made to the Donors of the American Chemical Society Petroleum Research Fund for support of this research.

References

Amin, M.H.G. et al., 1997. Study of flow and hydrodynamic dispersion in a porous medium using pulsed-field-gradient magnetic resonance. Proc. R. Soc. Lond. A 453, 489–513.

Balhoff, M.T., Thompson, K.E., 2006. A macroscopic model for shear-thinning flow in packed beds based on network modeling. Chem. Eng. Sci. 61 (2), 698–719.

Barbati, A.C., et al., 2016. Complex Fluids and Hydraulic Fracturing. In: Prausnitz, J. M. (Ed.) Annual Review of Chemical and Biomolecular Engineering, vol 7. pp. 415–453.

Berret, J.F., Lerouge, S., Decruppe, J.P., 2002. Kinetics of the shear-thickening transition observed in dilute surfactant solutions and investigated by flow birefringence. Langmuir 18 (20), 7279–7286.

Berret, J.F., 2006. Rheology of Wormlike Micelles: Equilibrium Properties and Shear Banding Transitions, in Molecular Gels. In: Weiss, R.G., Terech, P. (Eds.), Materials with Self-Assembled Fibrillar Networks. Springer, pp. 667–720.

Britton, M.M., Callaghan, P., 1997. Two-phase shear band structures at uniform stress. Phys. Rev. Lett. 78, 4930–4933.

Callaghan, P.T., 1991. Principles of Nuclear Magnetic Resonance Microscopy. Oxford University Press, New York.

Callaghan, P.T., 2011. Translational Dynamics and Magnetic Resonance: Principles of Pulsed Gradient Spin Echo NMR. Oxford University Press, New York.

Callaghan, P.T. et al., 1991. Diffraction-like effects in NMR diffusion studies of fluids in porous solids. Nature 351, 467–469.

Callaghan, P.T. et al., 1992. Diffusion in Porous systems and the influence of pore morphology in pulsed gradient spin echo nuclear magnetic resonance studies. J. Chem. Phys. 97 (1), 651–662.

Chaplain, V., Allain, C., Hulin, J.P., 1998. Tracer dispersion in power law fluids flow through porous media: evidence of a cross-over from a logarithmic to a power law behaviour. Europ. Phys. J. B 6 (2), 225–231.

Chen, C.M., Warr, G.G., 1997. Light scattering from wormlike micelles in an elongational field. Langmuir 13 (6), 1374–1376.

Chevalier, T., et al., 2014. Breaking of non-Newtonian character in flows through a porous medium. Phys. Rev. E, 89(2).

Chhabra, R.P., Comiti, J., Machac, I., 2001. Flow of non-Newtonian fluids in fixed and fluidised beds. Chem. Eng. Sci. 56 (1), 1–27.

Chu, Z.L., Dreiss, C.A., Feng, Y.J., 2013. Smart wormlike micelles. Chem. Soc. Rev. 42 (17), 7174–7203.

Codd, S.L. et al., 1999. Taylor dispersion and molecular displacements in poiseuille flow. Phys. Rev. E 60 (4), R3491–R3494.

Cokelet, G.R. et al., 2005. Magnetic Resonance Microscopy Determined Velocity and Hematocrit Distributions in a Couette Viscometer. Biorheology 42, 385–399.

Ernst, R.R., Bodenhausen, G., Wokaun, A., 1988. Principles of Nuclear Magnetic Resonance in One and Two Dimensions. Oxford University Press, Oxford.

Ezrahi, S., Tuval, E., Aserin, A., 2006. Properties, main applications and perspectives of worm micelles. Adv. Coll. Interface. Sci. 128, 77–102.

Feindel, K.W., Callaghan, P.T., 2010. Anomalous shear banding: multidimensional dynamics under fluctuating slip conditions. Rheol. Acta 49 (10), 1003–1013.

Fischer, P., Fuller, G.G., Lin, Z.C., 1997. Branched viscoelastic surfactant solutions and their response to elongational flow. Rheol. Acta 36 (6), 632–638.

Fukushima, E., 1999. Nuclear magnetic resonance as a tool to study flow. Annu. Rev. Fluid Mech. 31, 95–123.

Golombok, M., van der Wijst, R., 2013. Permeability thickening fluids for improved secondary oil recovery. J. Petrol. Sci. Eng. 110, 22–26.

Gonzalez, J.M. et al., 2005. The role of shear and elongation in the flow of solutions of semi-flexible polymers through porous media. Rheol. Acta 44 (4), 396–405.

Guillon, V. et al., 2014. Computing the longtime behaviour of NMR propagators in porous media using a pore network random walk model. Transp. Porous Media 101 (2), 251–267.

Guillon, V. et al., 2013. Superdispersion in homogeneous unsaturated porous media using NMR propagators. Phys. Rev. E 87 (4).

Haward, S.J. et al., 2012. Extensional rheology and elastic instabilities of a wormlike micellar solution in a microfluidic cross-slot device. Soft Matter 8 (2), 536–555.

Huang, C.C., Ryckaert, J.P., Xu, H., 2009. Structure and dynamics of cylindrical micelles at equilibrium and under shear flow. Phys. Rev. E 79 (4), 13.

Hunter, M.W., Callaghan, P.T., 2007. NMR measurement of nonlocal dispersion in complex flows. Phys. Rev. Lett. 99, 210602.

Johns, M.L. et al., 2003. Using MR techniques to probe permeability reduction in rock cores. AIChE J. 49 (5), 1076–1084.

Khrapitchev, A.A., Callaghan, P.T., 2003. Reversible and irreversible dispersion in a porous medium. Phys. Fluids 15 (9), 2649–2660.

Kubo, R., Toda, M., Hashitsume, N., 1991. Statistical Physics II: Nonequilibrium Statistical Mechanics. In: Fulde, P. (Ed.), Springer Series in Solid-State Sciences. vol. 31. Berlin: Springer-Verlag.

Lerouge, S., Berret, J.F., 2010. In: Dusek, K., Joanny, J.F. (Eds.), Shear-Induced Transitions and Instabilities in Surfactant Wormlike Micelles, in Polymer Characterization: Rheology, Laser Interferometry, Electrooptics 2010. Springer-Verlag Berlin: Berlin. pp. 1–71.

Lopez, X., Valvatne, P.H., Blunt, M.J., 2003. Predictive network modeling of single-phase non-Newtonian flow in porous media. J. Colloid Interface Sci. 264 (1), 256–265.

Lu, B. et al., 1998. Effect of chemical structure on viscoelasticity and extensional viscosity of drag-reducing cationic surfactant solutions. Langmuir 14 (1), 8–16.

Maier, R.S. et al., 2000. Pore-scale simulation of dispersion. Phys. Fluids 12, 2065–2079.

Maitland, G.C., 2000. Oil and gas production. Curr. Opin. Colloid Interface Sci. 5 (5–6), 301–311.

Manz, B., Alexander, P., Gladden, L.F., 1999. Correlations between dispersion and structure in porous media probed by nuclear magnetic resonance. Phys. Fluids 11 (2), 259–267.

Manz, B., Gladden, L.F., Warren, P.B., 1999. Flow and dispersion in porous media: Lattice-Boltzmann and NMR studies. AIChE J. 45 (9), 1845–1854.

Mertens, D. et al., 2006. Newtonian and non-Newtonian low Re number flow through bead packings. Chem. Eng. Technol. 29 (7), 854–861.
Metzler, R., Klafter, J., 2000. The random walk's guide to anomalous diffusion: a fractional dynamics approach. Phys. Rep. 339, 1–77.
Metzler, R., Klafter, J., 2001. Levy meets Boltzmann: strange initial conditions for Brownian and fractional Fokker-Planck equations. Phys. A 302, 290–296.
Muller, M., Vorwerk, J., Brunn, P.O., 1998. Optical studies of local flow behaviour of a non-Newtonian fluid inside a porous medium. Rheol. Acta 37 (2), 189–194.
Muller, A.J., Torres, M.F., Saez, A.E., 2004. Effect of the flow field on the rheological behavior of aqueous cetyltrimethylammonium p-toluenesulfonate solutions. Langmuir 20 (10), 3838–3841.
Neel, M.C., et al., 2011. All order moments and other functionals of the increments of some non-Markovian processes. J. Stat. Mech.-Theory Exper. p. P02066.
Odell, J.A., Haward, S.J., 2006. Viscosity enhancement in non-Newtonian flow of dilute aqueous polymer solutions through crystallographic and random porous media. Rheol. Acta 45 (6), 853–863.
Pearson, J.R.A., Tardy, P.M.J., 2002. Models for flow of non-Newtonian and complex fluids through porous media. J. Nonnewton. Fluid Mech. 102 (2), 447–473.
Prudhomme, R.K., Warr, G.G., 1994. Elongational flow of solutions of rodlike micelles. Langmuir 10 (10), 3419–3426.
Rojas, M.R., Muller, A.J., Saez, A.E., 2008. Shear rheology and porous media flow of wormlike micelle solutions formed by mixtures of surfactants of opposite charge. J. Colloid Interface Sci. 326 (1), 221–226.
Rothstein, J.P., 2003. Transient extensional rheology of wormlike micelle solutions. J. Rheol. 47 (5), 1227–1247.
Saffman, P.G., 1960. Dispersion due to molecular diffusion and macroscopic mixing in flow through a network of capillaries. J. Fluid Mech. 7 (2), 194–208.
Scheven, U.M. et al., 2007. A cumulant analysis for non-Gaussian displacement distributions in Newtonian and non-Newtonian flows through porous media. Magn. Reson. Imaging 25 (4), 513–516.
Scheven, U.M., Sen, P.N., 2002. Spatial and temporal coarse graining for dispersion in randomly packed spheres. Phys. Rev. Lett. 89 (25), 254501.
Scheven, U.M., Harris, R., Johns, M.L., 2007. Intrinsic dispersivity of randomly packed monodisperse spheres. Phys. Rev. Lett. 99 (5).
Sederman, A.J. et al., 1997. Magnetic resonance imaging of liquid flow and pore structure within packed beds. Chem. Eng. Sci. 52 (14), 2239–2250.
Seymour, J.D., Callaghan, P.T., 1996. "Flow-Diffraction" structural characterization and measurement of hydrodynamic dispersion in porous media by PGSE NMR. J. Magn. Reson., Ser. A 122, 90–93.
Seymour, J.D., Callaghan, P.T., 1997. Generalized approach to NMR analysis of flow and dispersion in porous medium. AIChE J. 43, 2096–2111.
Seymour, J.D. et al., 2004. Anomolous fluid transport in porous media induced by biofilm growth. Phys. Rev. Lett. 93 (19), 198103.
Sheppard, S., et al., 2002. Magnetic resonance imaging study of complex fluid flow in porous media: flow patterns and quantitative saturation profiling of amphiphilic fracturing fluid displacement in sandstone cores. in 6th International Conference on the Recent Advances in Magnetic Resonance Applications to Porous Media. 2002. Ulm, Germany: Elsevier Science Inc.
Shlesinger, M.F., Zaslavsky, G.M., Klafter, J., 1993. Strange kinetics. Nature 363, 31–37.
Song, Y.Q. et al., 2008. Magnetic resonance in porous media: Recent progress. J. Chem. Phys. 128 (5), 12.
Sridhar, T. et al., 1991. Measurement of extensional viscosity of polymer solutions. J. Nonnewton. Fluid Mech. 40 (3), 271–280.
Stapf, S. et al., 1998. Spatial correlations and dispersion for fluid transport through packed glass beads studied by pulsed field-gradient NMR. Phys. Rev. E 58 (5), 6206–6221.
Stejskal, E.O., Tanner, J.E., 1965. Spin diffusion measurements: Spin echoes in the presence of a time-dependent field gradient. J. Chem. Phys. 42, 288.
Stepisnik, J., 1985. Measuring and imaging of flow by NMR. Progr. NMR Spectros. 17, 187–209.
Sullivan, S.P. et al., 2007. Verification of shear-thinning LB simulations in complex geometries. J. Nonnewton. Fluid Mech. 143 (2–3), 59–63.
Sullivan, S.P., Gladden, L.F., Johns, M.L., 2006. Simulation of power-law fluid flow through porous media using lattice Boltzmann techniques. J. Nonnewton. Fluid Mech. 133 (2–3), 91–98.
van Santvoort, J., Golombok, M., 2016. Sweep enhancers for oil recovery. J. Petrol. Explor. Prod. Technol. 6 (3), 473–480.
Walker, L.M., Moldenaers, P., Berret, J.F., 1996. Macroscopic response of wormlike micelles to elongational flow. Langmuir 12 (26), 6309–6314.
Yang, J., 2002. Viscoelastic wormlike micelles and their applications. Curr. Opin. Colloid Interface Sci., 276–281
Yesilata, B., Clasen, C., McKinley, G.H., 2006. Nonlinear shear and extensional flow dynamics of wormlike surfactant solutions. J. Nonnewton. Fluid Mech. 133 (2–3), 73–90.
Zhao, Y., Shen, A.Q., Haward, S.J., 2016. Flow of wormlike micellar solutions around confined microfluidic cylinders. Soft Matter 12 (42), 8666–8681.